Discrete dislocation dynamics simulations of nanoindentation with pre-stress

Song, Hengxu; Yavas , Hakan; van der Giessen, Erik; Papanikolaou, Stefanos

Published in:
Journal of the Mechanics and Physics of Solids

DOI:
10.1016/j.jmps.2018.09.005

Publication date:
2019

Discrete Dislocation Dynamics Simulations of Nanoindentation with Pre-stress: Hardness and Statistics of Abrupt Plastic Events

H. Song, H. Yavas[a], E. Van der Giessen[b], S. Papanikolaou[a,b,c,*]

[a]*Department of Mechanical Engineering, Johns Hopkins University, Baltimore, MD, United States*
[b]*Zernike Institute for Advanced Materials, University of Groningen, 9747 AG Groningen, the Netherlands*
[c]*West Virginia University, Morgantown, WV, United States*

Abstract

Nanoindentation of crystalline materials has been thought as a primarily surface-driven technique that is not able to probe bulk mechanical properties directly, such as material yield strength or bulk plastic flow rates. We elucidate this question through extensive discrete dislocation plasticity simulations of nanoindentation on a single crystal. We consider the competition between nanoindentation and tensile loading (pre-stress) towards crystal plasticity. For this purpose, we study a two-dimensional discrete dislocation model where indentation is performed by using cylindrical indentation with varying radius under both displacement and load control. We focus on the behavior of the hardness and pop-in event statistics during nanoindentation under various pre-stress levels and we correlate them to the spatially correlated dislocation microstructure behavior. At small indentation depths (relative to other microstructural or tip length scales), we find that the hardness is inversely dependent on the plastic strain/dislocation density induced by the applied tensile pre-stress; consequently, we argue that small-depth indentation may be useful for identifying bulk plastic yielding behavior prior to indentation. In contrast, for larger indentation depths, pre-stress has no effect on hardness. However, effect of pre-stress can be revealed through plastic events statistics, both in load and displacement controlled protocols. Moreover, post-indentation surface morphology clearly shows the effect of the pre-stress.

1. Introduction

Indentation has been one of the major techniques towards identifying mechanical behavior of a vast list of materials. As a technique, it may be labeled as a direct probe, since there is an application of an explicit mechanical force towards identifying a deformation. Tabor (1951), for example, found that the yield strength σ_Y of a rigid perfectly-plastic material can be determined from the indentation hardness H as $\sigma_Y = H/C$, where the value of C is around 3, depending on the indenter geometry (Johnson, 1970). Especially during the last few decades, indentation has developed into an important means to interrogate size dependent plasticity. At the microscale, the Indentation Size Effect (ISE) has been primarily attributed to the plastic strain gradients that are induced by indentation (Nix and Gao, 1998), similar to strain gradients in bending and torsion. These strain gradients have been found to be the essential reason behind the adage "smaller is harder" (Aifantis, 1999; Pharr et al., 2010). Several strain gradient plasticity theories (e.g., Fleck et al., 1994; Gao et al., 1999; Huang et al., 2004) have been formulated that can capture the size effects in indentation and many other inhomogeneous deformation processes (Wei and Hutchinson, 1997; Huang et al., 2000; Xue et al., 2002; Song et al., 2016b).

However, compression experiments on micro and nanopillars uncovered that size effects are present even in the absence of strain gradients (Uchic et al., 2002, 2004; Dimiduk et al., 2005, 2007; Greer et al., 2005). Such

*Corresponding author
Email address: stefanos.papanikolaou@mail.wvu.edu (S. Papanikolaou)

size effects are responsible for strengthening at the nanoscale, and are shown to have various origins, such as dislocation source length truncation (Parthasarathy et al., 2007), dislocation starvation (Greer et al., 2005; Greer and Nix, 2006) and single-arm dislocation sources (Oh et al., 2009; Cui et al., 2014).

At the same time, it has become clear that mechanical response (stress-strain curve) at sub-micron length scales is intermittent. The intermittency (bursts of plastic deformation) displays size effects as well (Dimiduk et al., 2005; Ng and Ngan, 2008; Papanikolaou et al., 2011, 2012, 2017b). They are observed either as stress drops (when imposing displacement control) or strain jumps (when imposing load control) (Papanikolaou et al., 2017a; Sethna et al., 2017; Maass and Derlet, 2018). In load controlled indentation, intermittency (burst of the indentation depth) is also known as "pop-in" (Lorenz et al., 2003; Bradby et al., 2004), and in recent years, the first pop-in event in relatively pristine crystals (Durst et al., 2006; Shim et al., 2008) has been identified to mark the transition from elasticity to plasticity. Following the trend of size effects at the nanoscale, the equivalent stress for the first pop-in is also size dependent: Morris et al. (2011) proposed a statistical model for pop-in during nanoindentation that explained the size-dependence of pop-in stresses in accordance with experimental results. Moreover, Xia et al. (2016) extended pop-in investigations into multiple types of pop-in modes: a primary pop-in with a large displacement excursion and a number of subsequent pop-ins with comparable and small displacement excursions. The distribution of pop-ins in single FCC crystals has also been investigated to some degree (Wang et al., 2012) for Cu single crystals, finding that the distribution can be fitted by a Gaussian with mean and variance that depend on grain orientation.

It is common in indentation testing that the sample is kept on a stage without any pre-existing applied stresses. However, pre-application of stress can actually be used to estimate residual stress (Suresh and Giannakopoulos, 1998; Swadener et al., 2001; Lee and Kwon, 2004; Jang et al., 2003). The procedures for this are inspired by the observations of Tsui et al. (1996), revealing the effect of elastic tensile/compressive pre-stress on the measured hardness in microindentation experiments. The increase of tensile pre-stress resulted in a decrease of the measured hardness up to 6%, while the effect of compressive pre-stress was barely seen. Later on, finite element simulations (Bolshakov et al., 1996) suggested that the hardness dependence on pre-stress might be due to the experimental procedures underestimating the indentation contact area. Moreover, in reality, residual stress often results from plastic deformation left after fabrication/manufacture process, therefore, the residual stress problem is more complicated than just the influence of the elastic stress. Plasticity needs to be taken into account and the target should be the detection of bulk plasticity that is related to the residual stress. In order to achieve this, the indentation depth needs to remain small to avoid massive nucleation of dislocations from the indenter tip (as a probe, it should not generate what it is probing). Therefore, nanoindentation at very small depth would be the only choice.

Nanoindentation comes in two flavours: load control and displacement control. In experiments, load controlled indentation is often preferred for its simplicity because it does not require any electronic feedback loop (VanLandingham, 2003; Minor et al., 2006). Discrete dislocation plasticity simulations of nanoindentation, on the other hand, are most easily performed for displacement control as the contact area in that case is defined directly by the geometry of the (rigid) indenter (Balint et al., 2006; Widjaja et al., 2005). It is suspected, however, that the hardness and pop-in statistics display differences between load and displacement control, since Cui et al. (2016, 2017) showed significant differences between strain control and stress control in 3D discrete dislocation simulations of nanopillar compression. In the latter case study, the two different loading modes give different strengths and different event (strain burst/stress drops) statistics. Ultimately, it is natural to inquire for analogous differences between various loading modes in nanoindentation.

In this paper, we perform 2D plane-strain discrete dislocation dynamics (2D DDD) simulations of nanoindentation. Two-dimensional studies are always an idealization of real indentation experiments, but when formulated and interpreted properly, such as for the Nix and Gao (1998) ISE scaling law, they can reveal important trends. The 2D DDD approach adopted here has been shown to capture intriguing aspects of plastic deformation at submicron length scales, such as the Hall-Petch effect (Balint et al., 2008) and the ISE (Balint et al., 2006; Widjaja et al., 2006). We aim to explore and understand the nature of ISEs at the nanometer scale, in relation to the dislocation microstructure which is related to residual stress. We carry out nanoindentation simulations of a single crystalline sample by both load and displacement controlled protocols. The residual stress and related plasticity is created

through uniaxial tension of the sample prior to indentation. We focus on an exhaustive statistical exploration of residual stress effect on indentation hardness and pop-in effects. The ultimate target of this work is to build the connection between material bulk properties (plasticity related to residual stress) and surface indentation (indentation at small depth) and to further guide 3D simulation studies and experimental studies.

The remainder of this paper is organized as follows: Section 2 describes the methodology of our 2D-DDD model for indentation. Section 3 explains the load controlled protocol and presents a comparison with the usual displacement controlled indentation (Widjaja et al., 2005). Section 4 presents simulation results of indentation hardness at different indentation depths, both for load controlled and displacement controlled protocols. In addition, we focus on the effect of residual on hardness. The effect of residual stress on the pop-in statistics is presented in Section 5. In Section 6, we discuss and summarize our results.

2. Description of the problem

The model problem is shown in Fig. 1. A 2D crystal sample is indented by a rigid circular indenter (representing cylindrical indentation in 3D) of radius R at the middle of the sample. A macroscopic tensile stress with magnitude Σ is assigned at two ends of the sample prior to indentation. For large enough Σ, the system will generate dislocations (plasticity), and the indentation simulation is started once a stable dislocation microstructure has been formed. The finite element mesh is highly refined in the region close to the indenter with the element segment

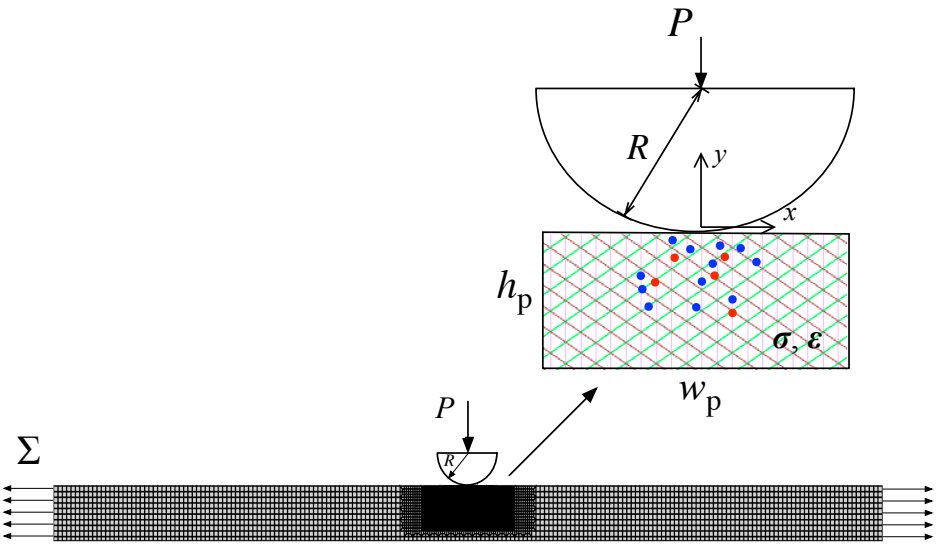

Figure 1: Schematic of indentation problem. The zoom in shows three slip systems (with different colors), red dots stand for dislocation sources while blue dots present dislocation obstacles.

length being $0.005R$ to accurately capture the evolution of the contact area. Inspired by the observation by Lee et al. (2005) that the indentation response for spherical indenters is insensitive to the friction coefficient, we assume that the contact between the rigid indenter and the crystal is perfectly sticking. This greatly simplifies the contact algorithm, since the contact area is determined only by the shape of the indenter and the roughness of the surface. The bottom is traction free, with the bottom central point of the geometry is fixed to prevent rigid move of the sample. Plasticity is limited to a plastic window with size $w_p = 20\mu$m and $h_p = 10\mu$m for computational efficiency; once a dislocation reaches the lateral or bottom borders of the plastic window, the simulation is stopped. The indented surface (top border of the plastic window) is transparent to dislocations, i.e., dislocations can escape the crystal through that surface and leave surface steps. Inside the plastic window, three slip systems are considered,

with slip directions at ±30° and 90° respectively, relative to the horizontal direction. Slip planes are spaced at $10b$ relatively to each other where b = 0.25nm is the magnitude of the Burgers vector. Dislocation sources (indicated by red dots in Fig. 1) and obstacles (indicated by blue dots) are randomly distributed on the slip planes. In order to further reduce the computational cost, dislocation sources are distributed in an even smaller window of 2μm by 2μm under the indenter, since dislocation sources far away from the indenter are barely influenced by indentation. Obstacles are distributed all over the plastic window.

Plastic deformation of the crystalline sample is described using the discrete dislocation framework for small strains developed by Van der Giessen and Needleman (1995), where the determination of the state in the material employs superposition. As each dislocation is treated as a singularity in a linear elastic background solid with Young's modulus E and Poisson's ratio ν, whose analytical solution is known at any position, this field needs to be corrected by a smooth image field ($\hat{}$) to ensure that actual boundary conditions are satisfied. Hence, the displacements u_i, strains ε_{ij}, and stresses σ_{ij} are written as

$$u_i = \tilde{u}_i + \hat{u}_i,\ \varepsilon_{ij} = \tilde{\varepsilon}_{ij} + \hat{\varepsilon}_{ij},\ \sigma_{ij} = \tilde{\sigma}_{ij} + \hat{\sigma}_{ij}, \tag{1}$$

where the ($\tilde{}$) field is the sum of the fields of all N dislocations in their current positions, i.e.

$$\tilde{u}_i = \sum_{J=1}^{N} \tilde{u}_i^{(J)},\ \tilde{\varepsilon}_{ij} = \sum_{J=1}^{N} \tilde{\varepsilon}_{ij}^{(J)},\ \tilde{\sigma}_{ij} = \sum_{J=1}^{N} \tilde{\sigma}_{ij}^{(J)}. \tag{2}$$

The image fields, indicated by the superposed $\hat{}$, are smooth and are obtained by solving a linear elastic boundary value problem using finite elements with the boundary conditions changing as the dislocation structure evolves under the application of mechanical load.

At the beginning of the calculation (before pre-stressing the sample), the crystal is stress and dislocation free. This corresponds to a perfectly-annealed sample, yet with pinned dislocation segments left that can act either as dislocation sources (Frank Read sources) or as obstacles. Dislocations are generated from sources when the resolved shear stress τ at the source location is sufficiently high (τ_{nuc}) for a sufficiently long time (t_{nuc}), thus mimicking the Frank-Read multiplication process in two dimensions.

We only consider bulk sources. The bulk sources are randomly distributed over slip planes at a density ρ_{nuc}, while their strength is selected randomly from a Gaussian distribution with mean value $\bar{\tau}_{\text{nuc}}$ = 50 MPa and 10% standard deviation. The effect of the initial dislocation structure distribution is still the frontier of fundamental research in discrete dislocation dynamics. For example, Madec et al. (2002); Bulatov et al. (2006); Sills et al. (2017) try to correlate dislocation microstructure to strain hardening. In our model, we choose to use the simplest random structure that obeys a Gaussian distribution. The sources are designed to mimic the Frank-Read mechanism in two dimensions, such that they generate a dipole of dislocations at distance L_{nuc}, when activated (Van der Giessen and Needleman, 1995). The initial distance between the two dislocations in the dipole is

$$L_{\text{nuc}} = \frac{E}{4\pi(1-\nu^2)} \frac{b}{\tau_{\text{nuc}}}, \tag{3}$$

at which the shear stress of one dislocation acting on the other is balanced by the local shear stress.

Once nucleated, the life of a dislocation is governed by the Peach-Koehler force acting on it. During its motion, a dislocation can either exit the sample through the traction-free sides, annihilate with a dislocation of opposite sign when their mutual distance is less than $6b$ or become pinned by an obstacle. Point obstacles are included merely to take into account that the glide of dislocations in single crystals can be impeded for various reasons. 2D point obstacles cannot be mapped one-to-one to physical objects, but rather represent the "mean" effect of small precipitates or of forest dislocations on out-of-plane slip systems which are not explicitly described in 2D model. Because of the ambiguous physical origin, the properties of 2D obstacles are very simple: they are randomly distributed over the slip planes; once a dislocation moves to the obstacle site (determined by the obstacle density), it is pinned there until its Peach-Koehler force exceeds the obstacle-dependent value $\tau_{\text{obs}}b$, after which the dislocation gets de-pinned. Detailed characteristics such as the stress field of a precipitate, the

thermally activated motion to by-pass the obstacle or the dwell time at an obstacle are not incorporated in a simple "mean" pinning/de-pinning model. Chakravarty and Curtin (2010) have shown in detail how dislocation sources and obstacles conspire in setting the yield strength and the hardening rate of a crystal. Under their assumption of very strong obstacles, the dislocations piling-up in front of an obstacle are so dense and long that they can be described by a continuum pile-up model, leading to a concrete prediction for the yield strength as a function of source strength, obstacle strength and the mean spacing between obstacles (Chakravarty and Curtin, 2010). In this, and earlier, work we have used much lower values of the obstacle strength, which do not give rise to long pile-ups but to a more uniform distribution of dislocations. The value used here is $\tau_{\text{obs}} = 150$ MPa on average with 20% standard deviation; together with an obstacle density that is eight times the source density gives rise to realistic size effects and dislocation densities in a previous nanopillar compression study (Papanikolaou et al., 2017b).

Dislocations are considered to move by glide only, driven by the component of the Peach-Koehler force in the slip direction. For the Ith dislocation, this force is given by

$$f^{(I)} = \boldsymbol{n}^{(I)} \cdot \left(\hat{\boldsymbol{\sigma}} + \sum_{J \neq I} \tilde{\boldsymbol{\sigma}}^{(J)} \right) \cdot \boldsymbol{b}^{(I)}, \tag{4}$$

where $\boldsymbol{n}^{(I)}$ is the slip plane normal and $\boldsymbol{b}^{(I)}$ is the Burgers vector of dislocation I. This force will cause the dislocation I to glide, following over-damped dynamics, with an instantaneous velocity

$$v^{(I)} = \frac{f^{(I)}}{B}, \tag{5}$$

governed by the drag coefficient B. In this paper, its value is taken as $B = 10^{-4}$Pa s, which is representative for aluminum. The values of Young's modulus and Poisson's ratio, $E = 70$ GPa, $\nu = 0.33$, are also characteristic for aluminum, but it bears emphasis that our crystal is a model material. Nevertheless, earlier studies with similar parameter values have shown to be able to capture small-scale dislocation-mediated plasticity in a variety of deformation problems (Nicola et al., 2003; Deshpande et al., 2005; Nicola et al., 2006; Balint et al., 2008; Shishvan and Van der Giessen, 2010; Song et al., 2016a; Papanikolaou et al., 2017b) including indentation (Balint et al., 2006; Widjaja et al., 2006, 2007).

Each sample contains a random distribution of bulk dislocation sources as well as dislocation obstacles; for each parameter study, we therefore studied 20 realizations. The simulation is carried out in an incremental manner, using a time step that is a factor 20 smaller than the nucleation time $t_{\text{nuc}} = 10$ ns. At the beginning of every time increment, nucleation, annihilation, pinning at and release from obstacle sites are evaluated. After updating the dislocation structure, the new stress field in the sample is determined, using the finite element method to solve for the image fields (Van der Giessen and Needleman, 1995).

3. Nanoindentation with load control protocol

In displacement controlled indentation, plasticity is characterized by a reduction of the indentation force, as seen in previous DD simulations (Balint et al., 2006; Widjaja et al., 2007). Contact between rigid indenter and crystal is sticky. Rather than adopting the simple projected contact area, we use the real contact area a computed as the total length of all finite elements that are in contact (*cf.* Widjaja et al., 2007).

In indentation experiments that are typically carried out using load control, plasticity is characterized by displacement bursts (pop-in), see e.g. (Suresh et al., 1999; Bei et al., 2005; Pathak et al., 2014). A real load controlled indentation simulation needs a contact algorithm to be implemented between indenter and sample, which would add significant complexity to the numerical implementation. In order to avoid this, we here propose a hybrid loading protocol to mimic the load control protocol used in experiments. The hybrid protocol is essentially displacement controlled based, but with a feedback loop to the indentation rate in order to maintain the indentation force until the indentation force increases. As in load controlled indentation, the position of indenter is adjusted and the indentation force never drops. The assumption in our hybrid protocol is that the indenter can move as fast

as needed in order to maintain the load level. By contrast, when studying indentation force drops under displacement control, we use a fixed displacement rate of 0.004 ms^{-1}. This indentation rate is much smaller than the one (0.1 ms^{-1}) used in previous indentation studies (Balint et al., 2006; Widjaja et al., 2007) to avoid the suppression of force drops by very high displacement rates, see Appendix for more details.

A comparison between load controlled indentation and displacement controlled indentation using an indenter with radius $R = 1\,\mu$m is shown in Fig. 2. It can be seen in Fig. 2(a) that the load controlled protocol gradually

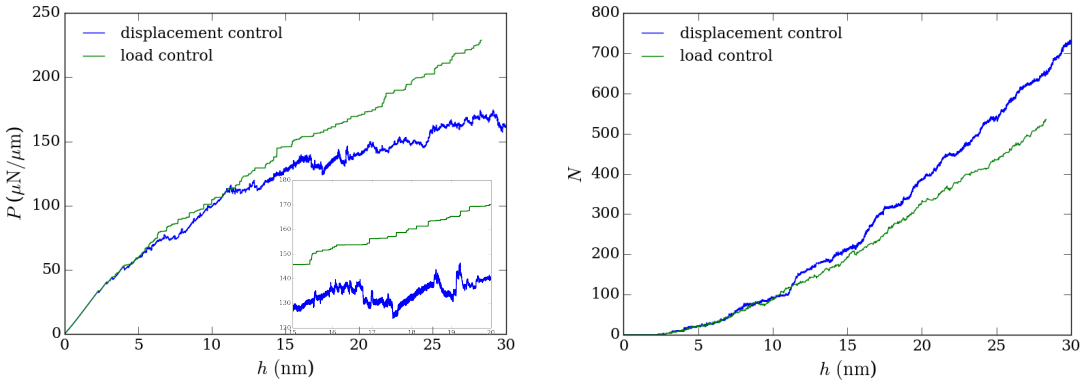

(a) (b)

Figure 2: Comparison between load controlled protocol and displacement controlled protocol with dislocation source density $\rho_{\mathrm{nuc}} = 75/\mu\mathrm{m}^2$. Two different protocols have the same initial dislocation structure (dislocation sources and obstacles), (a) indentation force – depth curves, (b) evolution of the total number of dislocations.

gives rise to a larger indentation force. The reason is that our load control protocol uses a higher displacement rate when the indentation force tends to drop and that a higher displacement rate yields a higher indentation force. The inset is the zoom in of the curve between indentation depth 15 nm and 20 nm. It can be clearly seen that plasticity is presented as displacement burst under load control while it is force drop under displacement control. The difference on the total number of dislocation can be seen in Fig. 2(b). At small indentation depth, the two protocols have more or less the same number of dislocations, but due to the changing displacement rate (a higher rate), application of the load control protocol gradually leads to fewer dislocations.

Details on the effect of the load control protocol are discussed in the Appendix. The different loading protocols are also discussed through nano pillar compression, a problem where the contact area stays constant.

4. Dependence of indentation hardness on pre-stress

Tsui et al. (1996) observed that a tensile pre-stress below the yield strength has a very small influence on the measured hardness in micron-indentation. In this study, we therefore use a tensile pre-stress that is large enough to trigger plasticity in order to see the influence of dislocation structure on the hardness measured subsequently by nano-indentation. The yield strength of the sample for given dislocation parameters (ρ_{nuc}, ρ_{obs}, τ_{nuc}, τ_{obs}) can be computed by either a force or displacement controlled tensile (or compression) simulation (see Appendix). However, since plasticity is confined to a plastic window that is smaller than the sample for computational efficiency, the yield strength cannot be obtained from the macroscopic stress Σ. An estimate of the yield strength can be obtained by first noting that for the chosen slip system orientations (cf. Fig. 1), the ratio between the critical resolved shear stress τ_{Y} and the initial tensile yield stress is $\tau_{\mathrm{Y}}/\sigma_{\mathrm{Y}} = \frac{1}{2}\sin 60^\circ$. The critical resolved shear stress is controlled by the weak dislocation sources in the Gaussian distribution with mean value $\bar{\tau}_{\mathrm{nuc}} = 50$ MPa and 10% standard deviation. Assuming τ_{Y} to be somewhere between one and a half standard deviation below the mean source strength, we find $\sigma_{\mathrm{Y}} \approx 100$MPa. This indeed is the value found for the simulations with $\rho_{\mathrm{nuc}} = 60\,\mu\mathrm{m}^{-2}$

in the Appendix. For the lowest source density considered in this study, $\rho_{\text{nuc}} = 15\,\mu\text{m}^{-2}$, the yield strength is likely to be somewhat larger, whereas for $\rho_{\text{nuc}} = 75\,\mu\text{m}^{-2}$ and $150\,\mu\text{m}^{-2}$ it may be somewhat lower. Some strain hardening caused by the high density of strong obstacles ensures a stable tensile response up to $\sigma_{\text{Y}} = 100$ MPa for the entire range of parameters used. Therefore, in this paper, the maximum tensile pre-stress Σ is set to be 100 MPa. For large enough tensile pre-stress, a dislocation structure and plastic strain will develop inside the plastic window, reducing the stress inside this region, while the rest of the sample remains elastic. The macroscopically applied tensile stress Σ, therefore, is not a good predictor of the residual stress and strain state inside the plastic window. Since the sources are distributed only inside the central 2μm by 2μm region, plastic deformation is not nominally homogeneous all over the plastic window, yet it is inside this effective plastic zone. The mean stress and strain state inside the effective plastic zone have been computed separately for various applied stresses and are listed in Table 1. In presenting the effect of pre-stress in the sequel, we therefore report the tensile stress σ and the tensile strain ε, both in the x-direction, averaged over the effective plastic zone. It bears emphasis that if the plastic window would span the entire specimen, σ would be equal to Σ.

Table 1: Information about state inside the plastic window in crystals with three dislocation source densities ρ_{nuc} at various levels of macroscopic pre-stress Σ (in MPa): the average tensile stress σ (in MPa), average tensile strain ε (in %), and average plastic strain ε^{p} in x-direction (in %), as well as dislocation density (ρ_{d} in μm^{-2}). Averages are computed over the 2μm by 2μm effective plastic zone centered underneath the indenter.

Σ \ ρ_{nuc}	$15\,\mu\text{m}^{-2}$				$75\,\mu\text{m}^{-2}$				$150\,\mu\text{m}^{-2}$			
	σ	ε	ε^{p}	ρ_{d}	σ	ε	ε^{p}	ρ_{d}	σ	ε	ε^{p}	ρ_{d}
0	0	0	0	0	0	0	0	0	0	0	0	0
10	10	0.012	0	0	10	0.012	0	0	10	0.012	0	0
20	20	0.025	0	0	20	0.025	0	0	20	0.025	0	0
30	30	0.038	0	0	30	0.038	0	0	30	0.038	0	0
40	40	0.054	0	0	40	0.054	0	0	40	0.054	0	0
50	45	0.066	0.0087	0.35	43	0.0675	0.0127	0.62	42	0.0685	0.015	3.1
80	68	0.11	0.023	3.25	63	0.115	0.034	8.5	57	0.1218	0.049	16.1
100	78	0.14	0.04	10.1	71	0.15	0.059	25.2	59	0.1796	0.104	38.1

We start indentation with the default indenter radius $R = 1\mu$m using the load control protocol on crystals with the default dislocation source density $\rho_{\text{nuc}} = 75/\mu\text{m}^2$. For the same sample (i.e., same dislocation source/obstacle distribution), the indentation force versus indentation depth ($P - h$ curve) with different pre-stresses is shown in Fig. 3. We observe that increasing the pre-tensile stress results in a decrease of the indentation force. One can expect this from an enhanced resolved shear stress argument, while at the same time, pre-stress induced dislocations will tend to accelerate the onset of yield.

4.1. Effect of pre-stress on hardness

Indentation hardness is defined as the indentation force P divided by the real contact area a. Fig. 4(a) shows examples of hardness versus indentation depth at various levels of tensile pre-stress. It can be seen that the hardness increases with indentation depth at small indentation depth just like without pre-stress as observed experimentally by Swadener et al. (2002) and in 2D DDD simulations by Widjaja et al. (2006). For readers who interpret the ISE as decrease in hardness with increasing indentation depth, it is important to note the experimentally confirmed difference between a wedge (Berkovich in 3D) and a circular (cylindrical in 3D) indenter: the ISE is controlled by indentation depth in Berkovich indentation whereas it is controlled by the indenter radius in spherical/cylindrical indentation. Moreover, the hardness actually increases with increasing depth for a spherical/cylindrical indenter, as will be seen in the future Fig. 8. Detailed discussions can be found in (Swadener et al., 2002; Widjaja et al., 2006).

With pre-stress, or rather pre-strain, Fig. 4(b) shows the hardness measured at different indentation depths. In order to provide a more direct connection to experimental studies, we plot the total tensile strain in the plastic

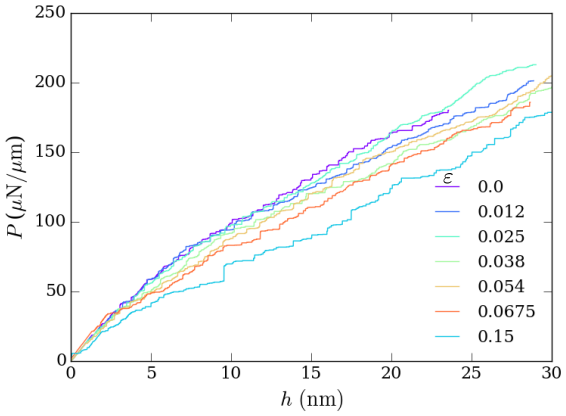

Figure 3: Examples of force – depth curves obtained under load controlled indentation of a pre-stressed sample containing source density of source density $\rho_{\text{nuc}} = 75/\mu\text{m}^2$. The legend stands for the mean tensile strain in the indented region prior to indentation, cf. Table 1.

window instead of the applied pre-stress. For the same indentation depth, we see that larger pre-strain reduces the indentation hardness; this is a small effect at low pre-strain but increasingly more at larger pre-strains. In fact, a transition is observed at pre-strains of around 0.06 to 0.07%, which is the moment at which yield happens (*cf.* Table 1). The effect of pre-stress changes with indentation depth, as can be clearly seen in Fig. 4(c) where the hardness is normalized by the hardness H_0 without pre-stress. We see that the hardness decreases with increasing pre-stress at small indentation depth, yet this trend becomes insignificant for indentation depths of 10 nm and above. This phenomenon is consistent with observations in our recent experimental study (Yavas et al., 2017). The hardness transition indicates that plasticity induced by pre-stressing of the sample can be detected by nanoindentation, and best so at small indentation depth. The influence of the pre-stress can also be revealed through the stress field under the indenter, shown in Fig. 5. Figures 5(a-b-c) give the stress field at different indentation depths when the tensile pre-stress is zero. We see that with increasing depth, dislocations get nucleated and a high-stress area extends inside the sample (recall that dislocations carry a singular stress field). By contrast, when the tensile pre-stress is 71 MPa, the stress field already fluctuates violently prior to indentation because of the dislocations generated during yield. Increasing the indentation depth changes the stress field, as can be seen in Fig. 5(d-e-f), but not as dramatically as in the case of zero pre-stress.

4.2. Effect of dislocation source density

It has been reported in many previous 2D DDD studies of different problems (Deshpande et al., 2005; Widjaja et al., 2006; Song et al., 2015) that the density of dislocation sources can restrict plasticity if the system does not have a surplus of dislocation sources. The computations at a source density $\rho_{\text{nuc}} = 75/\mu\text{m}^2$ reported above, reveal an effect of pre-stress on hardness. In this section, we report results for different dislocation source densities: $\rho_{\text{nuc}} = 15/\mu\text{m}^2$ and $\rho_{\text{nuc}} = 150/\mu\text{m}^2$. It is seen in the inset of Fig. 6(a) that the lower source density gives rise to the larger hardness at the same indentation depth, just like in the previous 2D DDD indentation study by Widjaja et al. (2006). Moreover, it is worthy to note that for the lower source density (Fig. 6(a)), the effect of pre-stress on hardness is still present at an indentation depth of 20 nm while the effect disappears for the highest source density (Fig. 6(b)).

As shown in Table 1, the effect of source density during pre-stressing is reflected in a different strain, plastic strain and dislocation density at the same macroscopic pre-stress. During indentation, source density will have an effect on dislocation nucleation as well. In order to exclude the effect of nucleation, we computed the hardness at a very small depth, of 0.5 nm, see Fig. 7(a). We see that the hardness is insensitive to the amount of pre-stress when still in the elastic regime, which is consistent with the findings of (Bolshakov et al., 1996). Above a pre-strain of

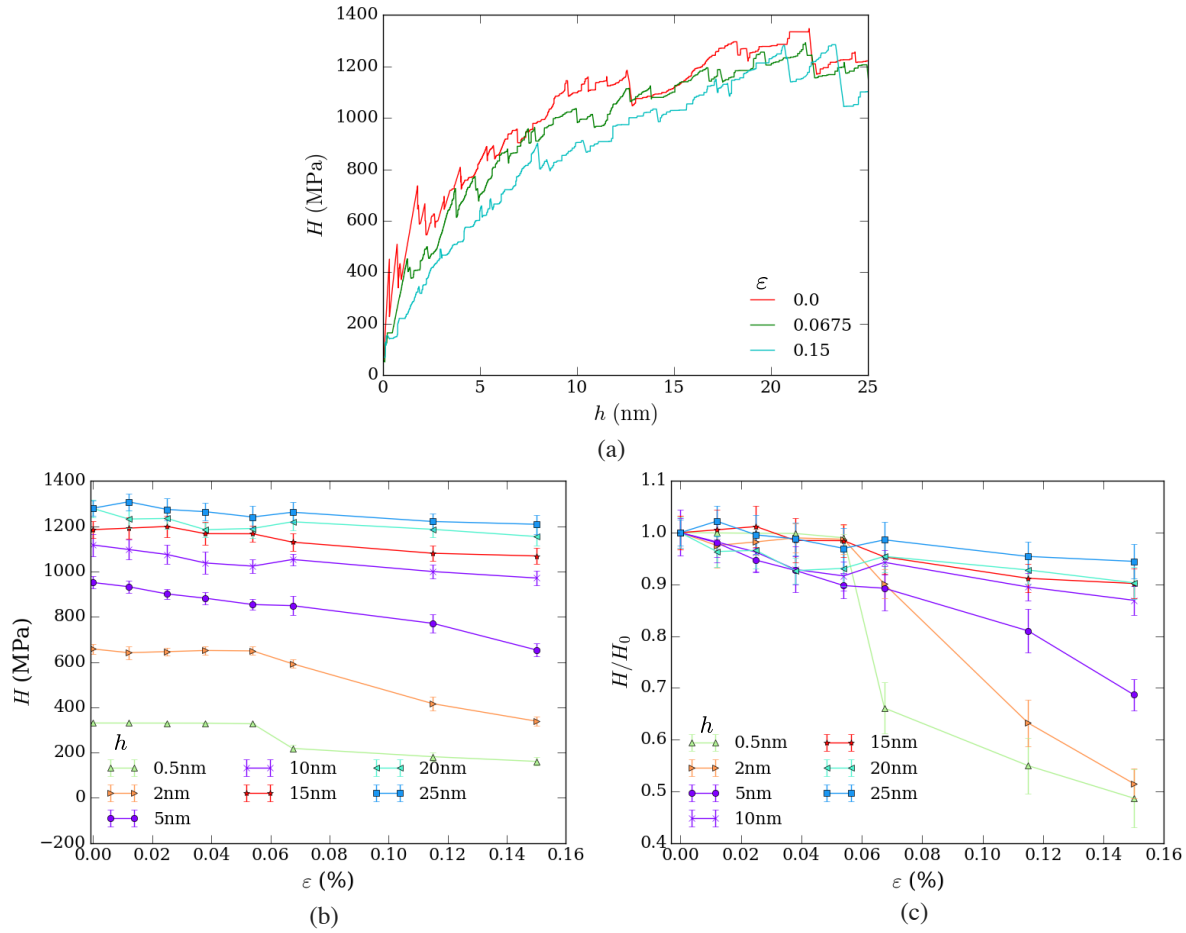

Figure 4: (a) Examples of hardness versus indentation depth curves for three different tensile pre-stress levels, obtained by load controlled protocol in a pre-stressed specimen with dislocation source density $\rho_{\text{nuc}} = 75/\mu\text{m}^2$. (b) Indentation hardness H at different indentation depths (indicated by the coloured symbols) for different levels of pre-strain, (c) hardness normalized by hardness H_0 without pre-stress. Error bars represent standard deviation of 20 realizations.

around 0.55% where yield had started, the hardness decreases with the amount of pre-strain for all source densities, but there is no clear correlation of H with ε. While the correlation between H and ε^{p} is found to be somewhat better, we find a convincing correlation in Fig. 7(b) between hardness with initial dislocation density irrespective of source density.

4.3. Effect of indenter radius

The results reported so far are for the default indenter radius $R = 1\mu$m used in this study; in Fig. 8 we present the results for a smaller indenter $R = 0.5\mu$m and for a larger indenter $R = 5\mu$m. It can be seen in the inset of Fig. 8(a) that at the same indentation depth, the smaller indenter gives rise to the larger hardness. This is consistent with the typical spherical/cylindrical indentation size effect (Swadener et al., 2002; Widjaja et al., 2006). Furthermore, we see that for a larger indenter, the hardness transition (decreasing hardness with increasing tensile pre-stress) disappears at a smaller indentation depth, *cf.* Fig. 8(a) and Fig. 8(b). This is related to dislocation nucleation

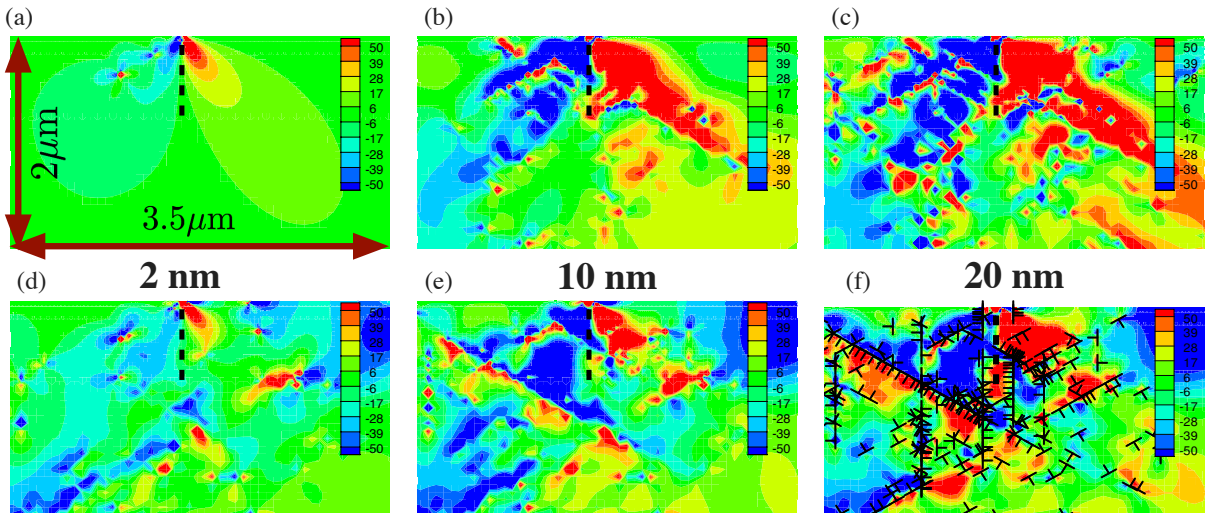

Figure 5: Shear stress field due to indentation in a crystal with $\rho_{\text{nuc}} = 75/\mu\text{m}^2$ for different tensile pre-stresses, inside a window of 3.5 μm by 2 μm centered below the indenter. (a), (b), (c) are for zero tensile pre-stress, (d), (e), (f) are the results with a pre-stress $\sigma = 71$MPa. Distributions are shown for different indentation depth as indicated between figures, (a) (d): 2 nm, (b) (e): 10 nm, (c) (f): 20 nm. (f) also contains dislocation structure. The thick dashed line indicates the indentation center.

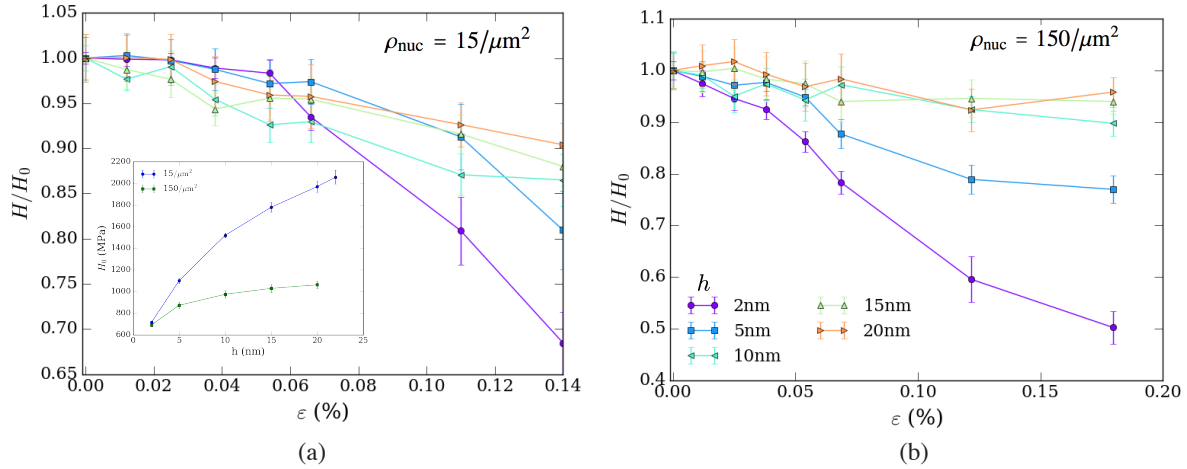

Figure 6: Normalized hardness (by hardness at 0 pre-stress) versus tensile pre-strain obtained by load controlled protocol for different dislocation source densities: (a) $\rho_{\text{nuc}} = 15/\mu\text{m}^2$, (b) $\rho_{\text{nuc}} = 150/\mu\text{m}^2$. The inset in (a) is the hardness at zero pre-stress as a function of indentation depth for two different dislocation source density. The different colours indicate the indentation depth h as specified in the legend of (b).

induced by the indenter: at the same indentation depth, the probability of dislocation nucleation is higher for a larger indenter.

4.4. Hardness measurement in displacement control

Fig. 9(a) shows the indentation force versus depth for displacement controlled indentation under different pre-stresses. Even though the difference in loading mode leads to the difference of indentation force depth curves, the effect of pre-stress on hardness is similar, see Fig. 9(b). Like under force controlled indentation, Fig. 7, the hardness at small depth correlates well with the dislocation density prior to indentation (results not shown). It should be

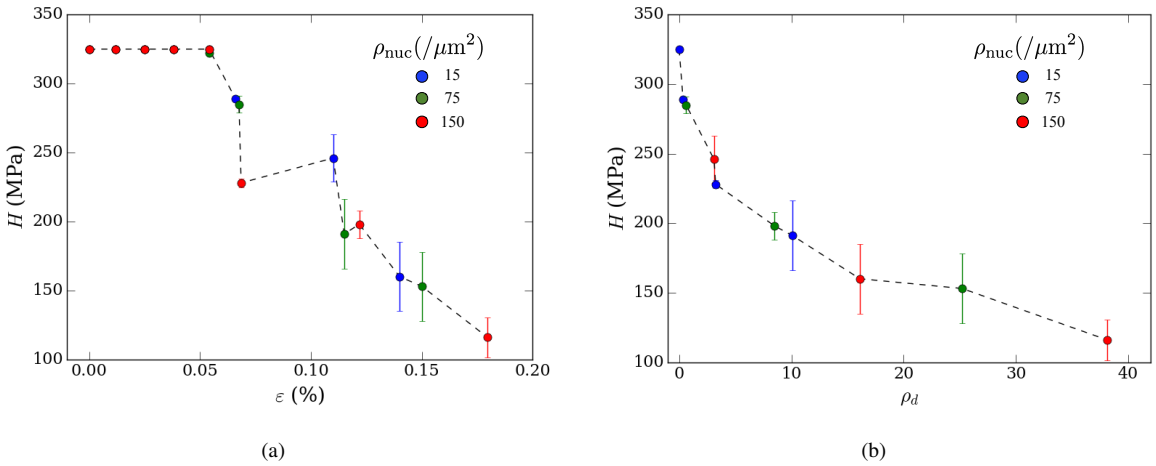

Figure 7: Hardness at indentation depth $h = 0.5$ nm for all three source densities considered, versus (a) the pre-strain and (b) dislocation density (in $\mu{\rm m}^{-2}$), *cf.* Table 1. The dashed lines merely serve as a guide to the eye.

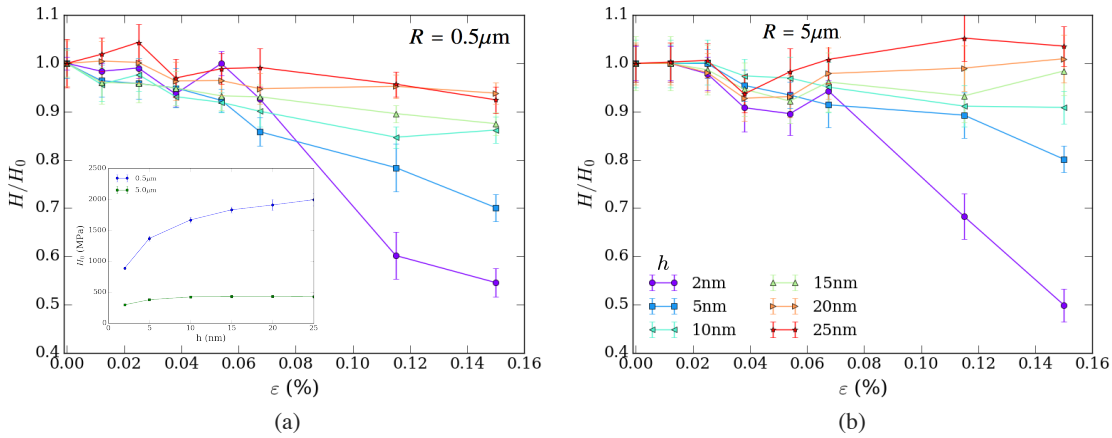

Figure 8: Normalized hardness (by hardness at 0 pre-stress) obtained by load controlled indentation of crystals having a dislocation source density $\rho_{\rm nuc} = 75/\mu{\rm m}^2$ as a function of the tensile pre-strain ε for an indenter with radius (a) $R = 0.5\mu$m, and (b) $R = 5\mu$m. The inset in (a) is the hardness with zero pre-stress at different depth for two different radii. Figure (a) and (b) share the legend shown in (b).

pointed out, however, that this initial dislocation density is slightly constrained by the size of the window in which dislocation sources are present. A few computations where sources were distributed over the entire plastic window, at the lowest source density of $\rho_{\rm nuc} = 15/\mu{\rm m}^2$, indicated that pre-stressing induced a higher dislocation density, but that the decay in hardness was similar to that shown in Fig. 7b, and in fact up to 10% more.

5. Pop-in statistics

When presenting our load control protocol for indentation in Sec. 3, we noted the difference in which plasticity reveals itself: as displacement jumps in load control versus force drops in displacement control. While the emphasis so far has been on the effect of pre-stress on the indentation hardness, in this section, we try to unveil the effect of pre-stress on the statistics of these signals of plasticity during indentation.

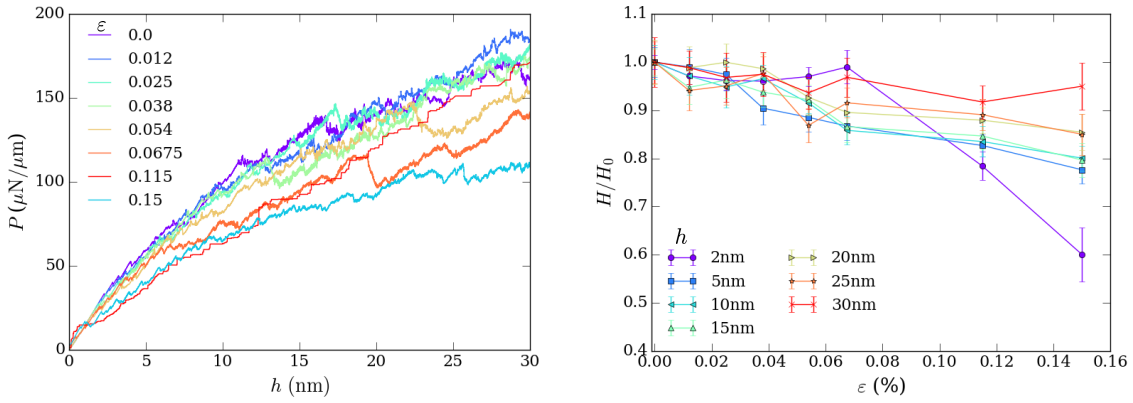

(a) (b)

Figure 9: Effect of pre-stress on hardness determined by displacement controlled indentation into a crystal with a dislocation source density $\rho_{\text{nuc}} = 75/\mu\text{m}^2$. (a) Indentation force – depth curves at various levels of pre-strain, (b) effect of pre-strain on normalized hardness as function of indentation depth.

In annealed crystals, the burst of indentation depth appearing during load control is normally called pop-in. In their experimental study, Morris et al. (2011) attributed the first pop-in to the nucleation of dislocations, while subsequent 3D DDD simulations by Chang et al. (2010) related this pop-in event to the fast multiplication of dislocations below the indenter. The initial dislocation structure in their computations is obtained from a molecular dynamics simulations of indentation. A similar procedure is not possible in a 2D analysis, but in our model, an initial dislocation structure is induced by tension prior to indentation.

Fig. 10(a) shows the average dislocation density ρ_{dis} over the entire plastic window ($20 \times 10\,\mu\text{m}^2$) at different indentation depths. It is seen that larger pre-stress introduces some dislocations, but the dislocation densities tend to approach each other at larger indentation depth irrespective of the pre-stress level. In order to see the connection between pop-ins and the nucleation of dislocations, we plot the rate of change of the dislocation density during indentation in Fig. 10(b). It can be clearly seen that at low pre-stress levels, the growth rate of dislocation density is higher, which means that dislocation nucleation (caused by indentation) is dominant. At high pre-stresses, plasticity is dominated by glide of the pre-stress induced dislocations.

The most straightforward way to unveil pop-in statistics is to analyze the displacement burst or the force drop in the indentation force-depth curve. The definition of a pop-in event is indicated in Fig. 11 on the response curves shown in the inset of Fig. 2(a): a displacement burst in force-controlled indentation is denoted by S_d while S is the force drop under load control. Figure 12 shows statistics of pop-in of samples (20 samples for each tensile pre-stress) under load control for the default dislocation source density $\rho_{\text{nuc}} = 75/\mu\text{m}^2$ and indenter tip radius $R = 1\mu\text{m}$, in terms of the probability density $P(S_d)$. Since we have seen a clear effect of pre-stress on the hardness in Fig. 4(b) at small depths, it is expected that the pop-in statistics also show some difference for varying pre-stresses. As can be seen in Fig. 12(a) where statistics are calculated for indentation up to a depth of 2 nm, the larger pre-stress (which leads to plasticity prior to indentation) gives rise to power law form statistical distributions with exponential cutoff. The exponent of around -1.5 is typical for events in dislocated systems, see e.g. the recent review by Papanikolaou et al. (2017a). When the statistics is gathered up to a larger indentation depth, such as 20 nm in Fig. 4(b), the effect of pre-stress on indentation hardness is so small that differences between pre-strain levels are barely visible.

Under the displacement controlled protocol, the signal of plasticity is a drop of the indentation force S as defined in Fig. 11. Since different pre-stress levels result in a different magnitude of indentation forces (*cf.* Fig. 9(a)), therefore the magnitude of S is expected to be different. In order to see statistics more clearly, we define the normalized event $S^* = S/(\delta s)_{\text{max}}$ and show the statistics of S^* in Fig. 13. In Fig. 13(a), statistics is done for

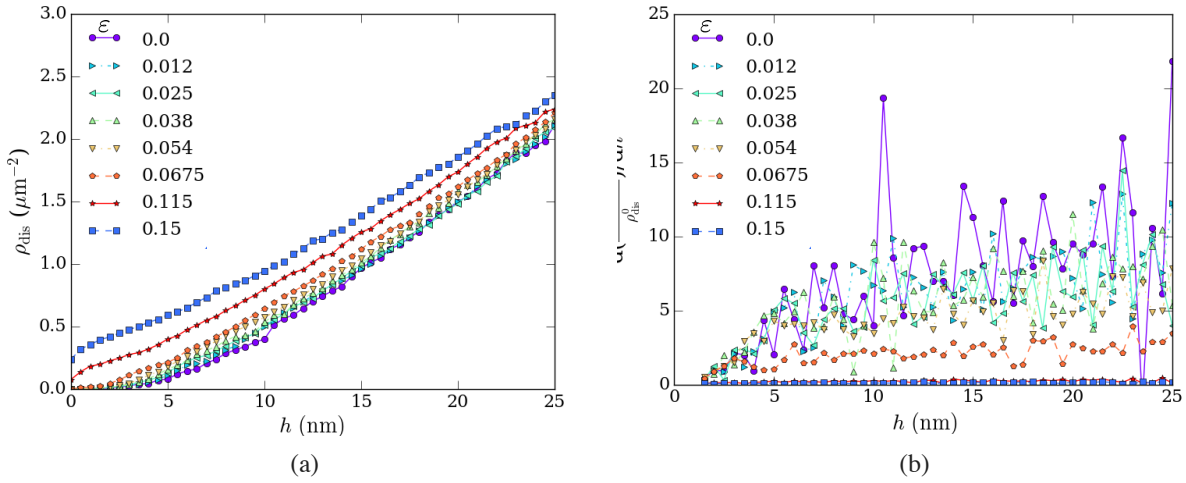

Figure 10: (a) Evolution of dislocation density during indentation in a crystal with $\rho_{\mathrm{nuc}} = 75/\mu\mathrm{m}^2$ after different levels of pre-stress. (b) change of dislocation density relative to the initial dislocation density ρ^0_{dis}. For large pre-stress, ρ^0_{dis} is determined by the pre-stress, for small pre-stress (no pre-stress induced dislocations), $\rho^0_{\mathrm{dis}} = 0.01/\mu\mathrm{m}^2$. The legends indicate the magnitude of the pre-strain (in %), *cf.* Table 1.

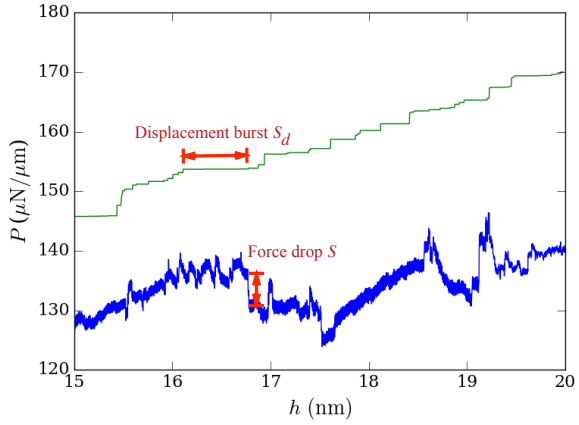

Figure 11: Definition of event. A displacement burst S_d in force-controlled indentation (green curve) is the accumulation of indentation depth increments δs_d until the force increases: $S_d = \sum_{i \in \text{eventsteps}} \delta s^i_d$. A force drop S in displacement-controlled indentation (blue curve) is the accumulation of incremental indentation force drops δs until the force increases: $S_d = \sum_{i \in \text{eventsteps}} \delta s^i$.

indentation depth up to 2 nm. It is clearly seen that statistics of larger pre-stresses (which leads to plasticity) is clearly distinguished with statistics of small pre-stresses. Through the difference becomes smaller when statistics is done for indentation depth up to 20 nm, shown in Fig. 13(b).

A subset of the events that lead to either force drops or displacement bursts is associated with the escape of dislocations through the free surface. It is well known that plastic straining tends to lead to surface roughening, but also indentation may lead to a permanent change of the surface morphology. To get some idea about the convolution of the two, we characterized the surface roughness after indentation (and unloading) into two samples with different amounts of pre strain. Surface roughness was characterized by the statistics of the surface slope, defined as $\chi_s = \langle (dy/dx)^2 \rangle - \langle dy/dx \rangle^2$. We found that after indentation up to a depth of $h = 8$ nm, the value of χ_s in

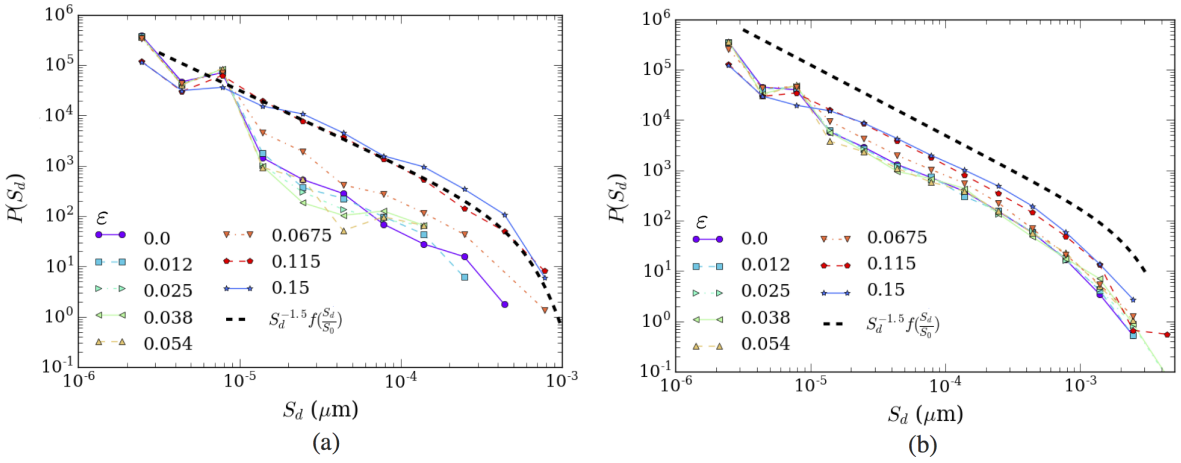

Figure 12: Probability event distribution $P(S_d)$ as function of event size S_d under different pre-stresses. Events statistics up to indentation depth (a) 2nm, and (b) up to 20nm. The dashed line is the power law fitting curve with the exponential cutoff S_0.

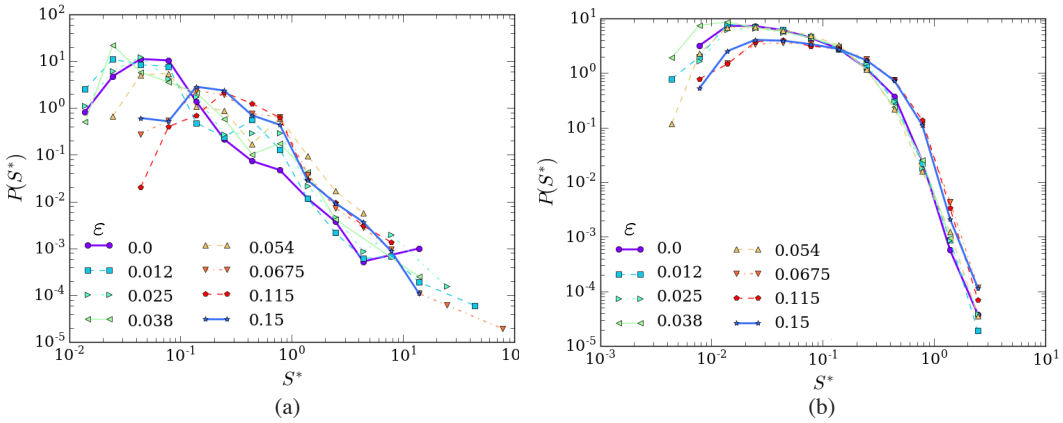

Figure 13: Statistics of indentation normalized force drops S^*, statistics of the smallest and largest pre-stress are in bold lines to guide the eye. (a) Events statistics up to indentation depth 2 nm, (b) events statistics up to indentation depth 20 nm.

the pre-strained sample (χ_s = 0.00065) is larger than without pre-strain (χ_s = 0.0002). What is more remarkable, however, is that after indentation up to h = 30 nm, the effect of pre-stress can still be observed (χ_s = 0.013 with pre-stress versus χ_s = 0.0085 without pre-stress) despite the fact that at this depth we no longer see an effect on hardness, *cf.* Fig. 4. This isolated observation may suggest that χ_s can perhaps be used in experiments to quantify pre-stress through post-indent surface morphology, but needs to be scrutinized further.

6. Discussion and Conclusions

The main focus of this paper is the effect of tensile pre-stress on the nanoindentation response (up to 40 nm depth) of single crystals. In principle, tensile pre-stress can have two effects on indentation: Firstly, as noted by Tsui et al. (1996), depending on the loading direction relative to the slip plane orientation, the applied pre-stress field can either interfere constructively with the indentation-induced stress field to enhance the resolved shear stress, or the opposite. This explains the difference in the effect of tensile versus compressive pre-stress, even

though the present 2D discrete dislocation plasticity model would not discriminate between the two in terms of dislocation density. The second effect of pres-stress enters through the density of dislocations that is produced prior to indentation at sufficiently high stress levels. These dislocations got pinned during pre-straining but, when their Burgers vector is favorably oriented, may become mobile during indentation because of the highly concentrated stress field induced by indentation. Tsui et al. (1996) have shown that if the pre-stress is within the elastic regime, there is almost no effect on the indentation hardness measured at a depth of hundreds of nanometers, which is in agreement with our computations (*cf.* Fig. 7(a)). At higher pre-stress levels, and for a given crystal orientation, we show that the effect of pre-stress found originates from the pre-stress induced plasticity/dislocations. The effect becomes less obvious or fades at depths where tension induced dislocations no longer dominate the indentation response, i.e., when dislocations nucleated by indentation govern plasticity.

It is important at this stage to recall that we have performed a 2D analysis, in which, contrary to the real 3D situation, dislocations cannot form junctions, Frank-Read segments or serve as forest dislocations. Instead, we distribute dislocation sources and obstacles as separate entities from dislocations. The consequence of this is that, in the absence of hard boundaries inside small volumes leading to extensive pile-ups, strain hardening in 2D-DDD is governed only by the obstacles that are present from the beginning. This is the reason why stress-strain curves obtained under strain control tend to show little hardening, see also Fig. 17c, despite the more or less linear growth of dislocation density. The 2D approach would need to be extended by special constitutive rules to represent 3D dislocation mechanisms before its predictions comply with the Taylor hardening law where the flow stress increases with the square root of the density of forest dislocations, as shown by Benzerga et al. (2003). With such an extension it is possible to recover Taylor hardening where the flow stress increases with the square root of the forest dislocation density. In the framework used here, these extra constitutive rules have not been incorporated, which explains why the small-depth indentation hardness decreases with the density of dislocations prior to indentation, as seen in Fig. 7(b).

The main target of this work has been to investigate the possibility of a bulk-dominated indentation regime in FCC crystals. We have shown that such a regime exists in the nanoscale, where a distinct transition in hardness is observed in the presence of pre-stress or, rather, prior plastic strain. This transition can be used for the identification of bulk mechanical properties: i.e., indentation in this regime (and only this regime) can be used to detect residual stress and its associated plasticity in a sample. Moreover, even though the effect on hardness fades with continued indentation, we have found that events statistics is always able to capture the influence of pre-stress.

In summary, the salient conclusions of this study are:

- Larger tensile pre-stress results in a smaller indentation hardness when the indentation depth is small (for the simulations conditions and model parameters used in this paper, a clear trend is observed when the depth is smaller than 5 nm).
- The indentation depth that influences the role of pre-stress depends on indenter geometry and material properties (source strength). The effect of pre-stress depends on the competition between pre-stress induced dislocations and indentation nucleated dislocations.
- Events statistics can capture the effect of pre-stress on indentation clearly for small indentation depth. Pop-in statistics in load controlled indentation shows a power law distribution with exponent around -1.5.

Acknowledgement

This research was supported by the U.S. Department of Energy, Office of Sciences, Basic Energy Sciences, DE-SC0014109. We also acknowledge the use of the Super Computing System (Spruce Knob) at WVU, which are funded in part by the National Science Foundation EPSCoR Research Infrastructure Improvement Cooperative Agreement 1003907, the state of West Virginia (WVEPSCoR via the Higher Education Policy Commission) and WVU. This work also benefited greatly from the facilities and staff of the High Performance Computing Center at the Zernike Institute for Advanced Materials at the University of Groningen, the Netherlands.

References

Aifantis, E.C. (1999), "Strain gradient interpretation of size effects." *International Journal of Fracture*, 95, 299–314.

Balint, D.S., V.S. Deshpande, A. Needleman, and E. Van der Giessen (2006), "Discrete dislocation plasticity analysis of the wedge indentation of films." *Journal of the Mechanics and Physics of Solids*, 54, 2281–2303.

Balint, D.S., V.S. Deshpande, A. Needleman, and E. Van der Giessen (2008), "Discrete dislocation plasticity analysis of the grain size dependence of the flow strength of polycrystals." *International Journal of Plasticity*, 24, 2149–2172.

Bei, H., E.P. George, J.L. Hay, and G.M. Pharr (2005), "Influence of indenter tip geometry on elastic deformation during nanoindentation." *Physical Review Letters*, 95, 045501.

Benzerga, A.A., Y. Bréchet, A. Needleman, and E. Van der Giessen (2003), "Incorporating three-dimensional mechanisms into two-dimensional dislocation dynamics." *Modelling and Simulation in Materials Science and Engineering*, 12, 159–196.

Bolshakov, A., W.C. Oliver, and G.M. Pharr (1996), "Influences of stress on the measurement of mechanical properties using nanoindentation: Part ii. finite element simulations." *Journal of Materials Research*, 11, 760–768.

Bradby, J.E., J.S. Williams, and M.V. Swain (2004), "Pop-in events induced by spherical indentation in compound semiconductors." *Journal of Materials Research*, 19, 380–386.

Bulatov, V.V., L.L Hsiung, M. Tang, A. Arsenlis, M.C. Bartelt, W. Cai, J.N. Florando, M. Hiratani, M. Rhee, G. Hommes, T.G. Pierce, and T.D. de la Rubia (2006), "Dislocation multi-junctions and strain hardening." *Nature*, 440, 1174.

Chang, H., M. Fivel, D. Rodney, and M. Verdier (2010), "Multiscale modelling of indentation in fcc metals: From atomic to continuum." *Comptes Rendus Physique*, 11, 285–292.

Chakravarty, S.S. and W.A. Curtin (2010), "Effect of source and obstacle strengths on yield stress: a discrete dislocation study." *Journal of the Mechanics and Physics of Solids*, 58, 625–635.

Cui, Y., P. Lin, Z. Liu, and Z. Zhuang (2014), "Theoretical and numerical investigations of single arm dislocation source controlled plastic flow in fcc micropillars." *International Journal of Plasticity*, 55, 279–292.

Cui, Y., G. Po, and N. Ghoniem (2016), "Controlling strain bursts and avalanches at the nano-to micrometer scale." *Physical Review Letters*, 117, 155502.

Cui, Y., G. Po, and N. Ghoniem (2017), "Influence of loading control on strain bursts and dislocation avalanches at the nanometer and micrometer scale." *Physical Review B*, 95, 064103.

Deshpande, V.S., A. Needleman, and E. Van der Giessen (2005), "Plasticity size effects in tension and compression of single crystals." *Journal of the Mechanics and Physics of Solids*, 53, 2661–2691.

Dimiduk, D.M., M.D. Uchic, and T.A. Parthasarathy (2005), "Size-affected single-slip behavior of pure nickel microcrystals." *Acta Materialia*, 53, 4065–4077.

Dimiduk, D.M., M.D. Uchic, S.I. Rao, C. Woodward, and T.A. Parthasarathy (2007), "Overview of experiments on microcrystal plasticity in fcc-derivative materials: selected challenges for modelling and simulation of plasticity." *Modelling and Simulation in Materials Science and Engineering*, 15, 135.

Durst, K., B. Backes, O. Franke, and M. Göken (2006), "Indentation size effect in metallic materials: Modeling strength from pop-in to macroscopic hardness using geometrically necessary dislocations." *Acta Materialia*, 54, 2547–2555.

Fleck, N.A., G.M. Muller, M.F. Ashby, and J.W. Hutchinson (1994), "Strain gradient plasticity: theory and experiment." *Acta Metallurgica et Materialia*, 42, 475–487.

Gao, H., Y. Huang, W.D. Nix, and J.W. Hutchinson (1999), "Mechanism-based strain gradient plasticityi. theory." *Journal of the Mechanics and Physics of Solids*, 47, 1239–1263.

Greer, J.R. and W.D. Nix (2006), "Nanoscale gold pillars strengthened through dislocation starvation." *Physical Review B*, 73, 245410.

Greer, J.R., W.C. Oliver, and W.D. Nix (2005), "Size dependence of mechanical properties of gold at the micron scale in the absence of strain gradients." *Acta Materialia*, 53, 1821–1830.

Huang, Y., S. Qu, K. Hwang, M. Li, and H. Gao (2004), "A conventional theory of mechanism-based strain gradient plasticity." *International Journal of Plasticity*, 20, 753–782.

Huang, Y., Z. Xue, H. Gao, W.D. Nix, and Z.C. Xia (2000), "A study of microindentation hardness tests by mechanism-based strain gradient plasticity." *Journal of Materials Research*, 15, 1786–1796.

Jang, J., D. Son, Y. Lee, Y. Choi, and D. Kwon (2003), "Assessing welding residual stress in a335 p12 steel welds before and after stress-relaxation annealing through instrumented indentation technique." *Scripta Materialia*, 48, 743–748.

Johnson, K.L. (1970), "The correlation of indentation experiments." *Journal of the Mechanics and Physics of Solids*, 18, 115–126.

Lee, Y. and D. Kwon (2004), "Estimation of biaxial surface stress by instrumented indentation with sharp indenters." *Acta Materialia*, 52, 1555–1563.

Lee, H., J.H. Lee, and G.M. Pharr (2005), "A numerical approach to spherical indentation techniques for material property evaluation." *Journal of the Mechanics and Physics of Solids*, 53, 2037–2069.

Lorenz, D., A. Zeckzer, U. Hilpert, P. Grau, H. Johansen, and H.S. Leipner (2003), "Pop-in effect as homogeneous nucleation of dislocations during nanoindentation." *Physical Review B*, 67, 172101.

Maass, R. and P.M. Derlet (2018), "Micro-plasticity and recent insights from intermittent and small-scale plasticity." *Acta Materialia*, 143, 338–363.

Madec, R., B. Devincre, and L.P. Kubin (2002), "From dislocation junctions to forest hardening." *Physical Review Letters*, 89, 255508.

Minor, A.M., S.S. Asif, Z. Shan, E.A. Stach, E. Cyrankowski, T.J. Wyrobek, and O.L. Warren (2006), "A new view of the onset of plasticity during the nanoindentation of aluminium." *Nature Materials*, 5, 697–702.

Morris, J.R., H. Bei, G.M. Pharr, and E.P. George (2011), "Size effects and stochastic behavior of nanoindentation pop in." *Physical Review Letters*, 106, 165502.

Ng, K. and A. Ngan (2008), "A monte carlo model for the intermittent plasticity of micro-pillars." *Modelling and Simulation in Materials Science and Engineering*, 16, 055004.

Nicola, L., E. Van der Giessen, and A. Needleman (2003), "Discrete dislocation analysis of size effects in thin films." *Journal of Applied Physics*, 93, 5920–5928.

Nicola, L., Y. Xiang, J.J. Vlassak, E. Van der Giessen, and A. Needleman (2006), "Plastic deformation of freestanding thin films: experiments and modeling." *Journal of the Mechanics and Physics of Solids*, 54, 2089–2110.

Nix, W.D. and H. Gao (1998), "Indentation size effects in crystalline materials: a law for strain gradient plasticity." *Journal of the Mechanics and Physics of Solids*, 46, 411–425.

Oh, S., M. Legros, D. Kiener, and G. Dehm (2009), "In situ observation of dislocation nucleation and escape in a submicrometre aluminium single crystal." *Nature Materials*, 8, 95–100.

Papanikolaou, S., F. Bohn, R.L. Sommer, G. Durin, S. Zapperi, and J.P. Sethna (2011), "Universality beyond power laws and the average avalanche shape." *Nature Physics*, 7, 316–320.

Papanikolaou, S., D.M. Dimiduk, W. Choi, J.P. Sethna, M.D. Uchic, C.F. Woodward, and S. Zapperi (2012), "Quasi-periodic events in crystal plasticity and the self-organized avalanche oscillator." *Nature*, 490, 517–521.

Papanikolaou, S., Y. Cui, and N. Ghoniem (2017a), "Avalanches and plastic flow in crystal plasticity: an overview." *Modelling and Simulation in Materials Science and Engineering*, 26, 013001.

Papanikolaou, S., H. Song, and E. Van der Giessen (2017b), "Obstacles and sources in dislocation dynamics: Strengthening and statistics of abrupt plastic events in nanopillar compression." *Journal of the Mechanics and Physics of Solids*, 102, 17–29.

Parthasarathy, T.A., S.I. Rao, D.M. Dimiduk, M.D. Uchic, and D.R. Trinkle (2007), "Contribution to size effect of yield strength from the stochastics of dislocation source lengths in finite samples." *Scripta Materialia*, 56, 313–316.

Pathak, S., J.L. Riesterer, S.R. Kalidindi, andJ. Michler (2014), "Understanding pop-ins in spherical nanoindentation." *Applied Physics Letters*, 105, 161913.

Pharr, G.M., E.G. Herbert, and Y. Gao (2010), "The indentation size effect: a critical examination of experimental observations and mechanistic interpretations." *Annual Review of Materials Research*, 40, 271–292.

Sethna, J.P., M.K. Bierbaum, K.A. Dahmen, C.P. Goodrich, J.R. Greer, L.X. Hayden, J.P. Kent-Dobias, E.D. Lee, D.B. Liarte, X. Ni, et al. (2017), "Deformation of crystals: Connections with statistical physics." *Annual Review of Materials Research*, 47.

Shim, S., H. Bei, E.P. George, and G.M. Pharr (2008), "A different type of indentation size effect." *Scripta Materialia*, 59, 1095–1098.

Shishvan, S.S. and E. Van der Giessen (2010), "Distribution of dislocation source length and the size dependent yield strength in freestanding thin films." *Journal of the Mechanics and Physics of Solids*, 58, 678–695.

Sills, R.B., N. Bertin, A. Aghaei, and W. Cai (2017), "Dislocation networks and the microstructural origin of strain hardening." *arXiv preprint arXiv:1712.00120*.

Song, H., V.S. Deshpande, and E. Van der Giessen (2016a), "Discrete dislocation plasticity analysis of loading rate-dependent static friction." *Proceedings of the Royal Society A*, 472, 20150877.

Song, H., R.J. Dikken, L. Nicola, and E. Van der Giessen (2015), "Plastic ploughing of a sinusoidal asperity on a rough surface." *Journal of Applied Mechanics*, 82, 071006.

Song, H., E. Van der Giessen, and X. Liu (2016b), "Strain gradient plasticity analysis of elasto-plastic contact between rough surfaces." *Journal of the Mechanics and Physics of Solids*, 96, 18–28.

Suresh, S. and A.E. Giannakopoulos (1998), "A new method for estimating residual stresses by instrumented sharp indentation." *Acta Materialia*, 46, 5755–5767.

Suresh, S., T.G. Nieh, and B.W. Choi (1999), "Nano-indentation of copper thin films on silicon substrates" *Scripta Materialia*, 41, 951–957.

Swadener, J.G., E.P. George, and G.M. Pharr (2002), "The correlation of the indentation size effect measured with indenters of various shapes." *Journal of the Mechanics and Physics of Solids*, 50, 681–694.

Swadener, J.G., B. Taljat, and G.M. Pharr (2001), "Measurement of residual stress by load and depth sensing indentation with spherical indenters." *Journal of Materials Research*, 16, 2091–2102.

Tabor, D. (1951), *The Hardness of Metals*, Clarendon Press, Oxford.

Tsui, T.Y., W.C. Oliver, and G.M. Pharr (1996), "Influences of stress on the measurement of mechanical properties using nanoindentation: Part i. experimental studies in an aluminum alloy." *Journal of Materials Research*, 11, 752–759.

Uchic, M.D., D.M. Dimiduk, J.N. Florando, and W.D. Nix (2002), "Exploring specimen size effects in plastic deformation of ni 3 (al, ta)." In *MRS Proceedings*, volume 753, BB1–4, Cambridge Univ Press.

Uchic, M.D., D.M. Dimiduk, J.N. Florando, and W.D. Nix (2004), "Sample dimensions influence strength and crystal plasticity." *Science*, 305, 986–989.

Van der Giessen, E. and A. Needleman (1995), "Discrete dislocation plasticity: a simple planar model." *Modelling and Simulation in Materials Science and Engineering*, 3, 689.

VanLandingham, M.R. (2003), "Review of instrumented indentation." *Journal of Research of the National Institute of Standards and Technology*, 108, 249.

Wang, W., Y. Zhong, K. Lu, L. Lu, D.L. McDowell, and T. Zhu (2012), "Size effects and strength fluctuation in nanoscale plasticity." *Acta Materialia*, 60, 3302–3309.

Wei, Y. and J.W. Hutchinson (1997), "Steady-state crack growth and work of fracture for solids characterized by strain gradient plasticity." *Journal of the Mechanics and Physics of Solids*, 45, 1253–1273.

Widjaja, A., A. Needleman, and E. Van der Giessen (2006), "The effect of indenter shape on sub-micron indentation according to discrete dislocation plasticity." *Modelling and Simulation in Materials Science and Engineering*, 15, S121.

Widjaja, A., E. Van der Giessen, V.S. Deshpande, and A. Needleman (2007), "Contact area and size effects in discrete dislocation modeling of

wedge indentation." *Journal of Materials Research*, 22, 655–663.
Widjaja, A., E. Van der Giessen, and A. Needleman (2005), "Discrete dislocation modelling of submicron indentation." *Materials Science and Engineering: A*, 400, 456–459.
Xia, Y., Y. Gao, G.M. Pharr, and H. Bei (2016), "Single versus successive pop-in modes in nanoindentation tests of single crystals." *Journal of Materials Research*, 31, 2065–2075.
Xue, Z., Y. Huang, and M. Li (2002), "Particle size effect in metallic materials: a study by the theory of mechanism-based strain gradient plasticity." *Acta Materialia*, 50, 149–160.
Yavas, H., H. Song, K.J. Hemker, and S. Papanikolaou (2017), "Detecting the plane-tension induced crystal plasticity transition using nanoindentation as a probe: Experiments and simulations." *Submitted*.

Appendix

In the main text, we have used a load controlled protocol for the indentation computations that involves changing the displacement rate (which is why we term it a hybrid approach) in order to prevent the force drop while the contact area evolves. Since discrete dislocation plasticity is inherently rate sensitive, the load controlled protocol gives rise to a larger indentation force and a smaller dislocation density than displacement control, *cf.* Fig. 2. In order to substantiate this, Fig. 14 shows results for displacement controlled indentation at different displacement rates. Fig. 14(a), (b) are results using a loading velocity 0.004 m s^{-1} for 10 samples, while Fig. 14(c), (d) are results for a higher loading velocity (0.1 m s^{-1}). The higher rate leads to the larger indentation force and smaller dislocation density at larger depth. At the same time, the response at higher loading velocity is smoother because the higher rate suppresses the force drops, as mentioned in the main text.

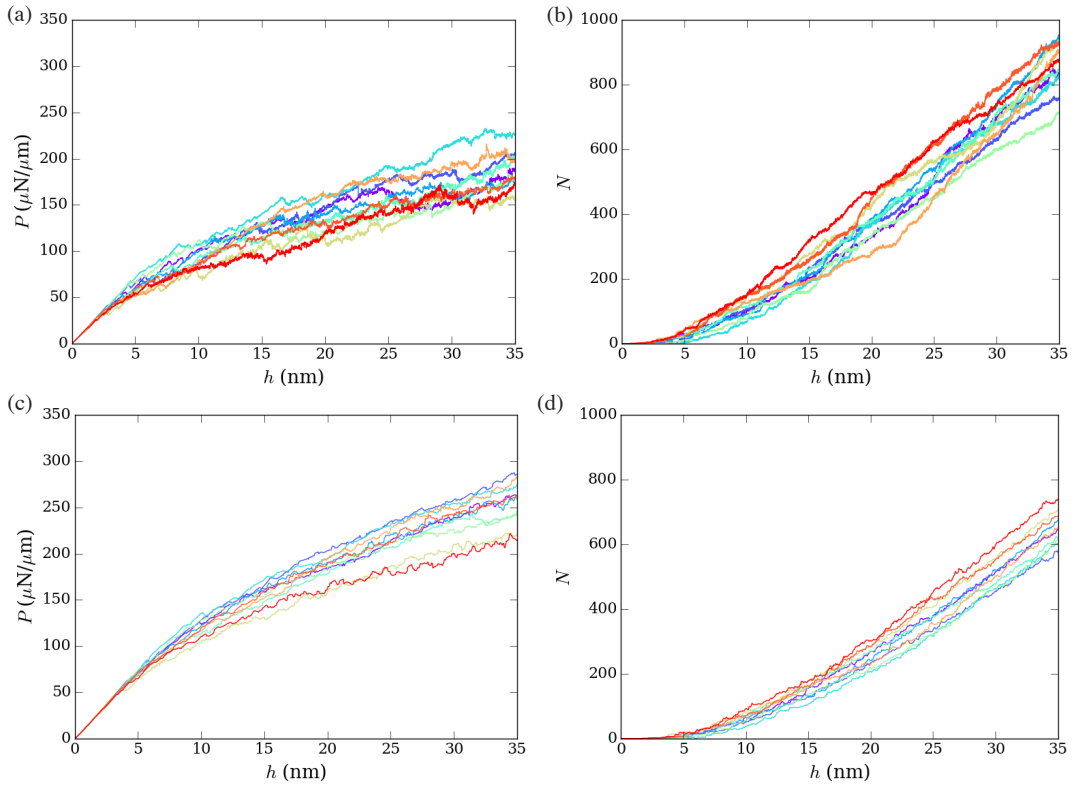

Figure 14: Displacement controlled indentation with different loading velocities. (a) Indentation force and (b) total number of dislocations versus indentation depth, at low loading velocity (0.004 ms^{-1}); (c) indentation force and (d) total number of dislocations versus indentation depth, at high loading velocity (0.1 ms^{-1}).

In order to verify our hybrid load controlled protocol, we apply the same protocol to nano pillar compression where the contact area remains constant, see Fig. 15. We consider only a single slip system with a slip spacing of $10b$; this problem is similar to that in (Papanikolaou et al., 2017b) but with only bulk dislocation sources. Three loading modes are considered. First, Fig. 16(a) shows stress versus strain curves of 10 samples using a stress controlled protocol. Here, the stress rate is kept constant at a value given by $\dot{\sigma} = E^*\dot{\varepsilon}$ determined by the same strain rate $\dot{\varepsilon} = 10^4\ \mathrm{s}^{-1}$ used in displacement controlled protocol, with $E^* := E/(1-\nu^2)$ being the plane strain tensile modulus. The result using displacement control (i.e., at constant strain rate) is shown in Fig. 16(b). Thirdly, the result of the hybrid stress controlled protocol is shown in Fig. 16(c). It is observed that the stress control protocol leads to more hardening than the displacement controlled protocol. Moreover, the stress controlled protocol (Fig. 16(a)) and the hybrid stress controlled protocol (Fig. 16(c)) have more or less the same average response.

At a much lower strain rate of $\dot{\varepsilon} = 10^2\ \mathrm{s}^{-1}$, we clearly see strain bursts when using stress controlled protocol (Fig. 17(a)), and large stress drops when using the displacement controlled protocol (Fig. 17(b)). Under the hybrid stress protocol (Fig. 17(c)) the strain bursts are not as clear as under stress control, due to the adapting strain rate, but the statistics of strain bursts, shown in Fig. 17(d), have a similar distribution. The main difference is that the hybrid stress control protocol suppresses big strain burst due to the higher strain rate used during iteration.

A stress controlled protocol is not possible for indentation because the stress state is not uniform underneath the indenter. Based on the observation that the average mechanical response during pillar compression as computed with the hybrid stress controlled protocol is almost the same as that obtained with the stress controlled protocol, we expect that our hybrid load controlled protocol is effective in indentation.

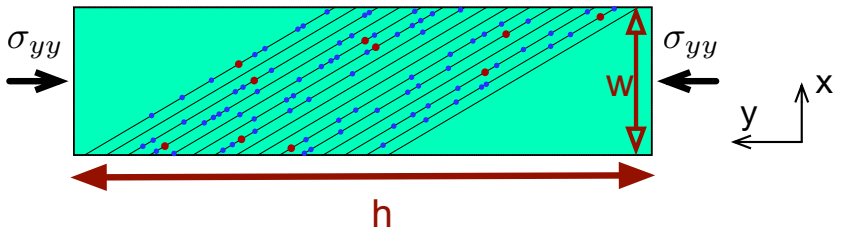

Figure 15: Schematic of pillar compression, $h = 4w = 2\mu$m, single slip system is used. Source (red dots) and obstacle (blue dots) densities are $\rho_{\mathrm{nuc}} = 60/\mu\mathrm{m}^2$ and $\rho_{\mathrm{obs}} = 480/\mu\mathrm{m}^2$ respectively.

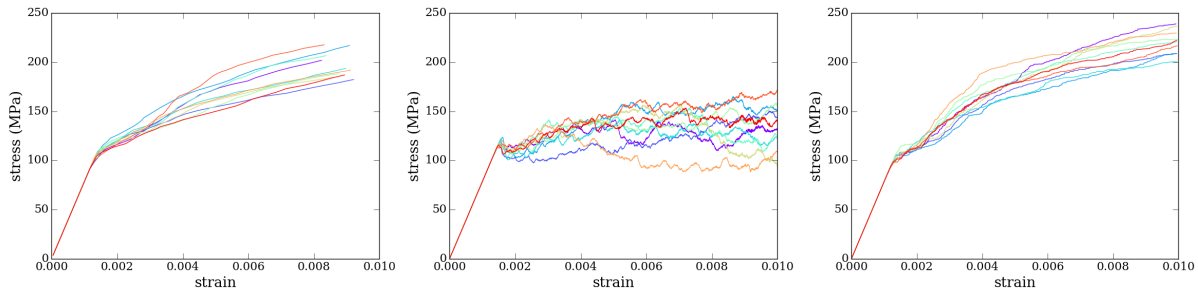

Figure 16: Pillar compression with different loading protocols at strain rate 10^4/s. (a) Stress control, (b) displacement control, (c) load control protocol used in indentation, (d) schematic of pillar compression, $h = 4w = 2\mu$m, single slip system is used. Source (red dots) and obstacle (blue dots) densities are $\rho_{\mathrm{nuc}} = 60/\mu\mathrm{m}^2$ and $\rho_{\mathrm{obs}} = 480/\mu\mathrm{m}^2$ respectively.

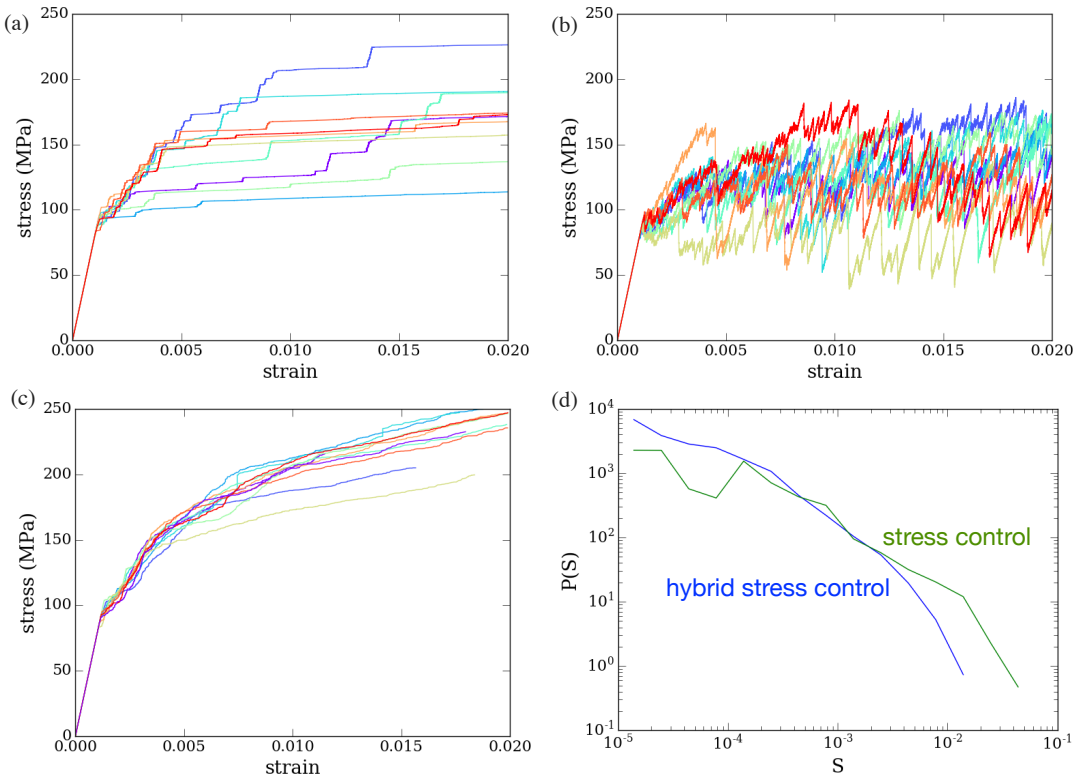

Figure 17: Pillar compression with different loading protocols at strain rate 10^2/s. (a) Stress control, (b) displacement control, (c) load control protocol used in indentation, (d) statistics of the strain bursts (*cf.* Fig. 11) in two different loading modes.